Supplementary Information

A High-Pressure Artificial Photosynthetic Device: Pumping Carbon Dioxide as well as Selectivity

Kai Deng,[1] Hao Feng,[1] Dong Liu,* Longfei Chen, Ying Zhang, Qiang Li*

MIIT Key Laboratory of Thermal Control of Electronic Equipment, School of Energy and Power Engineering, Nanjing University of Science and Technology, Nanjing 210094, China

[1]These authors contributed equally.

*Corresponding Authors: liudong15@njust.edu.cn; liqiang@njust.edu.cn.

Contents

1. Supplementary text

2. Supplementary Figures 1 to 12

3. Supplementary Tables 1 to 6

4. Supplementary references

Supplementary text

(1) XPS results of OP-Cu

The original and the fitted XPS spectra of OP-Cu (operated at 50 atm for one hour) were shown in Figure S5. Following the protocol reported in Biesinger [S1], Cu LMM spectrum of OP-Cu was fitted using spectrum of Cu^0 with seven peaks at 921.35 eV, 919.83 eV, 918.91 eV, 918.09 eV, 915.78 eV, 914.26 eV and 910.94 eV, and spectrum of Cu^{1+} with four peaks at 921.88 eV, 917.95 eV, 916.72 eV and 913.19 eV. Figure S5(c) shows the summation of fitted Cu^0 and Cu^{1+} LMM peaks that were used to calculate the Auger parameters listed in Table S3. Results show that the Auger parameters are 1851.55 eV for Cu^0 and 1849.40 eV for Cu^{1+}, which agree well with the values reported in Biesinger [S1] and Shima et al. [S2].

These results indicate the reduction from Cu^{1+} to Cu^0 (also proved by the XRD results in Figure 1) as well as the co-existence of Cu^0 and Cu^{1+}. Now, we comment on the effects of co-existence of Cu^0 and Cu^{1+} on CO_2R. First, both Li et al. [15] and Li and Kanan [32] reported that the presence of a thin, metastable Cu_2O layer cannot be ruled out. Secondly, we presented the original and the fitted XPS spectra of a Cu foil sample (99.9999%) in Figure S5 and calculated Auger parameters and atomic ratios shown in Table S3. Results also indicate the existence of Cu^{1+}. In addition, the Cu^0 ratios are very close for OP-Cu (~36%) and Cu foil (~38%). Thirdly, we performed OP-Cu-catalyzed PEC CO_2R reactions for 1, 4, 8 and 12 hours. Figure R3 shows that the yield of each product increases proportionally with time demonstrating the long-term stability of OP-Cu. We also presented the XPS results of OP-Cu operated at 50

atm for 12 hours in Figure S5 and Table S3. Therefore, we speculated that the co-existence of Cu^0 and Cu^{1+} was not the reason behind high CO_2R selectivity, although we cannot rule out the effect of Cu^{1+}.

(2) Generality of our proposed operational strategy

Preparation and characterization of Cu_2O precursor. The exact same method, reported in Li and Kanan [32], was used. Cu foil, purchased from Alfa Aesar, was first electro-polished; and then, it was annealed in a tube furnace at 130°C for 12 hours. XPS spectrum of the Cu_2O precursor was shown in Figures S9a and S9b. Results clearly indicated the presence of Cu^{1+}.

Referenced results. As a reference, the benchmark Cu catalyst (ref-Cu) was synthesized by electro-reduction of the Cu_2O precursor at 1 atm. Then, ref-Cu-catalyzed PEC CO_2R reaction was also performed at 1 atm. Figure S10 shows that the cathodic reduction is dominated by HER whose selectivity is higher than 93%. The selectivity is as low as 3% for both formate and CO production. These results agree well with those reported in Li and Kanan [32].

HiPAD results. To demonstrate the power and generality of our proposed operational strategy, the OP-Cu catalyst was synthesized by electro-reduction of the same Cu_2O precursor inside HiPAD. Then, the OP-Cu-catalyzed PEC CO_2R reaction straightly operated without making any changes to, nor taken anything in or out of HiPAD. The XPS spectra in Figures S9d and S9e indicated the presence of Cu^0 and Cu^{1+}. However, the peaks associated with Cu^{2+} in the spectrum for Cu_2O precursor were

absent. These results demonstrate the complete reduction of the Cu_2O film, although we cannot rule out the presence of a thin, metastable Cu_2O layer or other surface Cu^{1+} species during PEC CO_2R reaction. SEM images in Figures S9c and S9f show that the morphology of the Cu_2O precursor was intact after PEC CO_2R reaction. Both the XPS and SEM results reported here agree well with those reported in Li and Kanan [32]. Figure S10 shows the selectivity of each product for OP-Cu at 50 atm and 2.0 V working voltage between the photoanode and the cathode. Results show that the formate selectivity increases to as high as 22% and a near 4-fold enhancement of CO_2R selectivity was achieved compared to the referenced results.
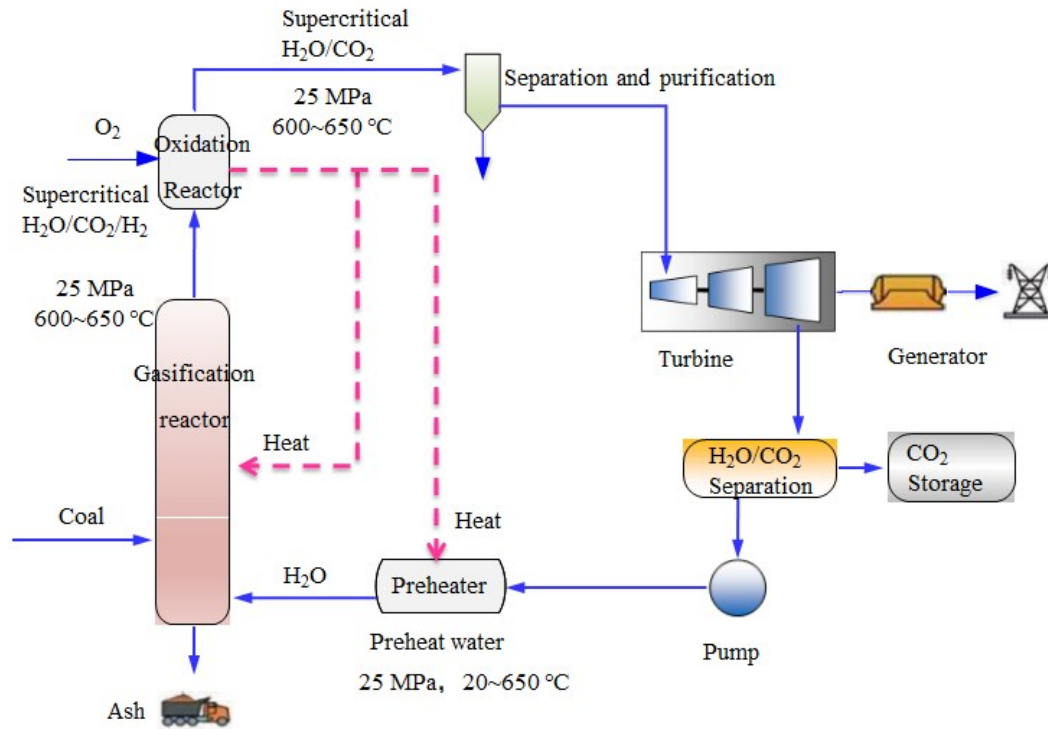
Figure S1. Schematic of the power generation system with coal gasified in supercritical water. This technology represents a potential pressurized CO_2 source. In this system, the coal is first gasified in supercritical water in the gasification reactor. By leveraging the unique properties of supercritical water, the organic matter in the coal is converted to H_2 and CO_2, and N, S, P, Hg and other elements are deposited as inorganic salt slag. Therefore, in contrast to conventional coal-fired power plants, NO_x, SO_x, PM 2.5 and other pollution productions are intrinsically eliminated in this system thereby avoiding the reduction of the system efficiency. Then, the supercritical $H_2O/CO_2/H_2$ mixture is oxidized in the oxidation reactor where H_2 is converted to H_2O with the generated heat used for the gasification reactor and the feed water preheater. After the oxidation reaction, the supercritical H_2O/CO_2 mixture drives a turbine to generate electricity. Finally, the exhaust H_2O and CO_2 are separated with H_2O circulated and CO_2 stored.

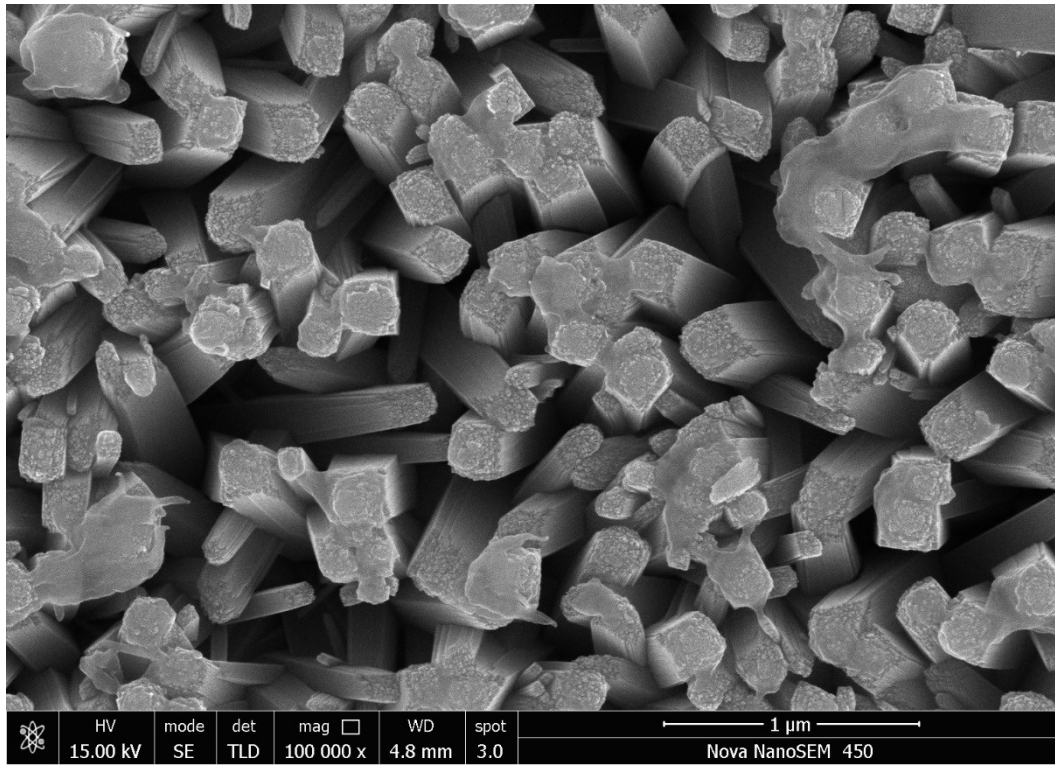| HV	mode	det	mag □	WD	spot	⊢————— 1 µm —————
15.00 kV	SE	TLD	100 000 x	4.8 mm	3.0	Nova NanoSEM 450

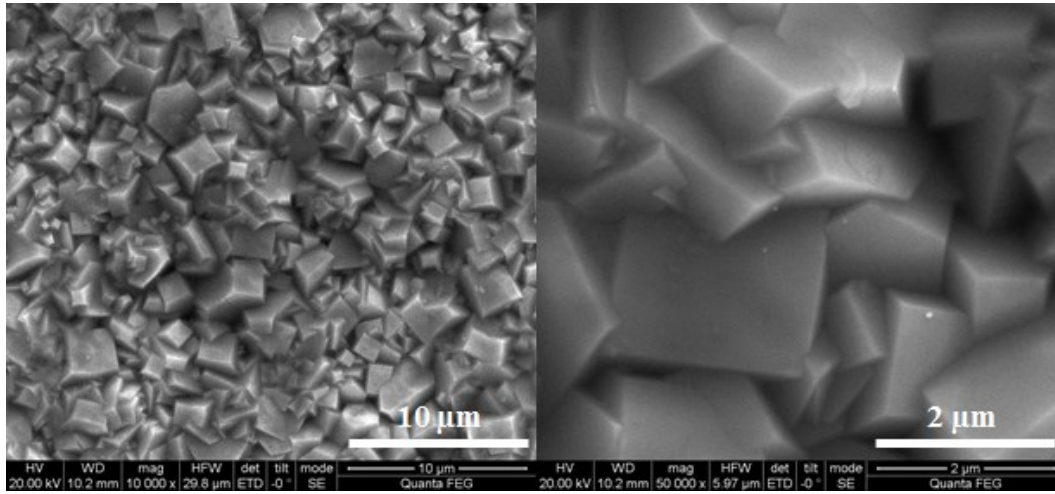**Figure S2.** SEM image of TiO$_2$ nanorod array photoanode.

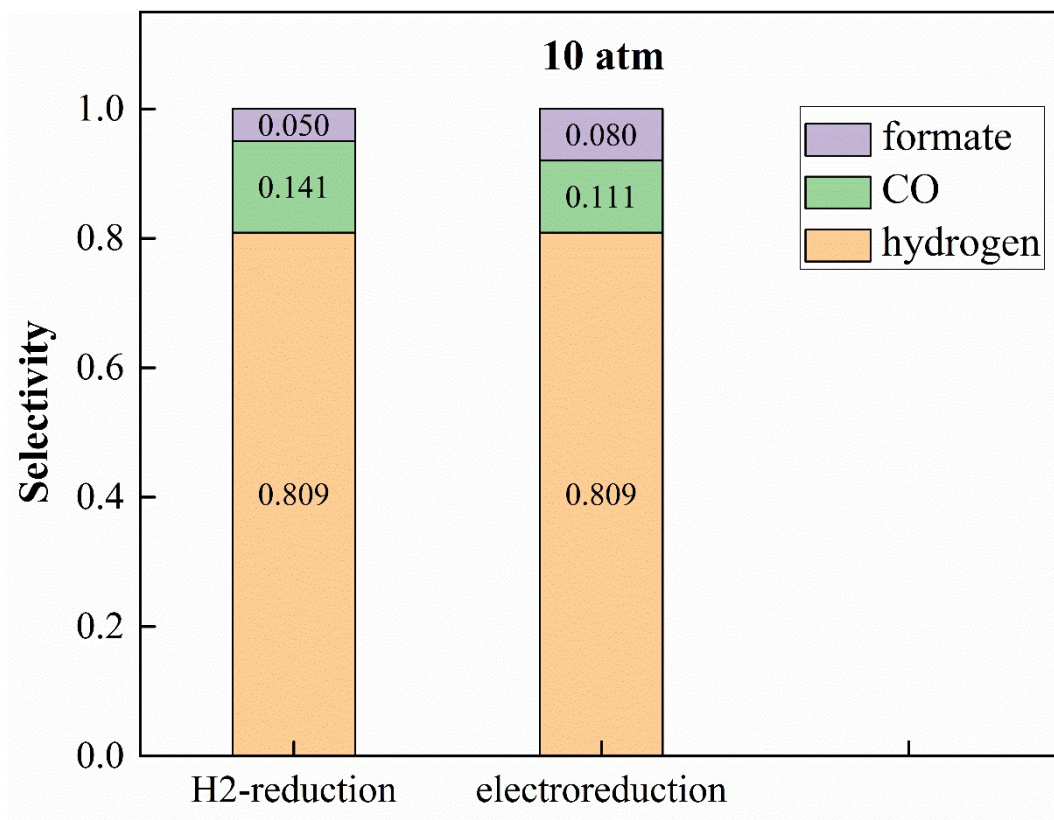**Figure S3.** Low-magnification (left) and high-magnification (right) SEM images of Cu_2O precursor.

Figure S4. Product selectivity of eSitu-Cu catalysts synthesized by reduction in H_2 atmosphere and by electroreduction for 10 atm.
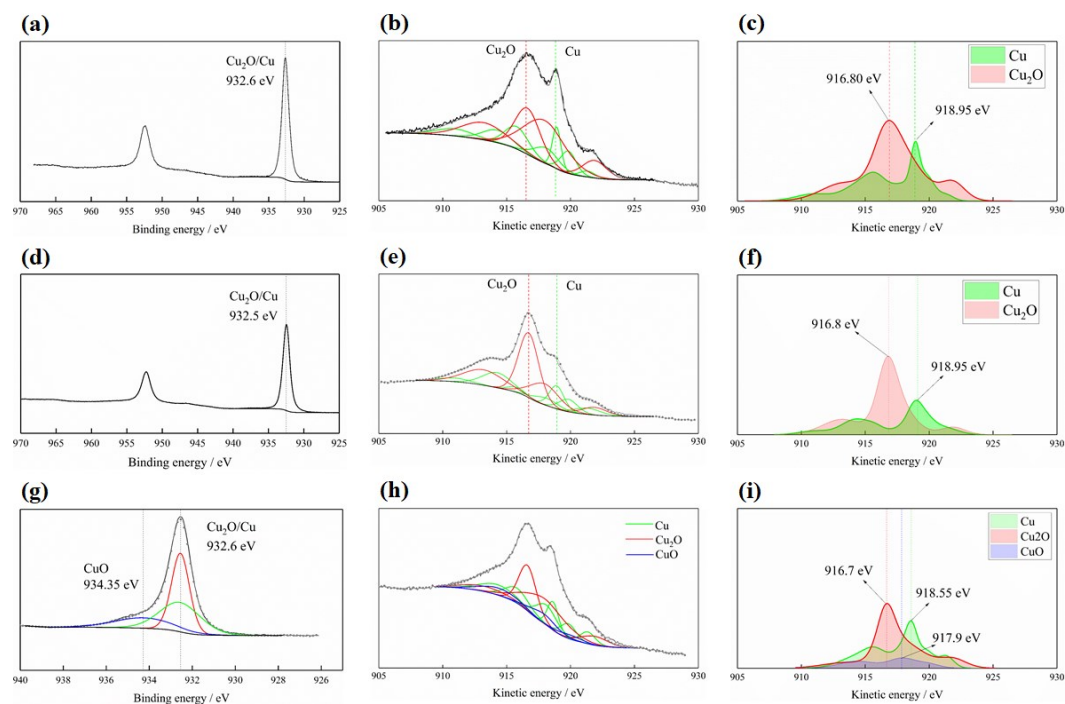
Figure S5. XPS spectra of OP-Cu and Cu foil. (a) Cu 2p, (b) original and fitted Cu LMM, and (c) summation of fitted Cu^0 and Cu^{1+} LMM peaks for OP-Cu operated at 50 atm for one hour. (d) Cu 2p, (e) original and fitted Cu LMM and (f) summation of fitted Cu^0 and Cu^{1+} LMM peaks for OP-Cu operated for 12 hours. (g) Cu 2p, (h) original and fitted Cu LMM, and (i) summation of fitted Cu^0, Cu^{1+} and Cu^{2+} LMM peaks for Cu foil.
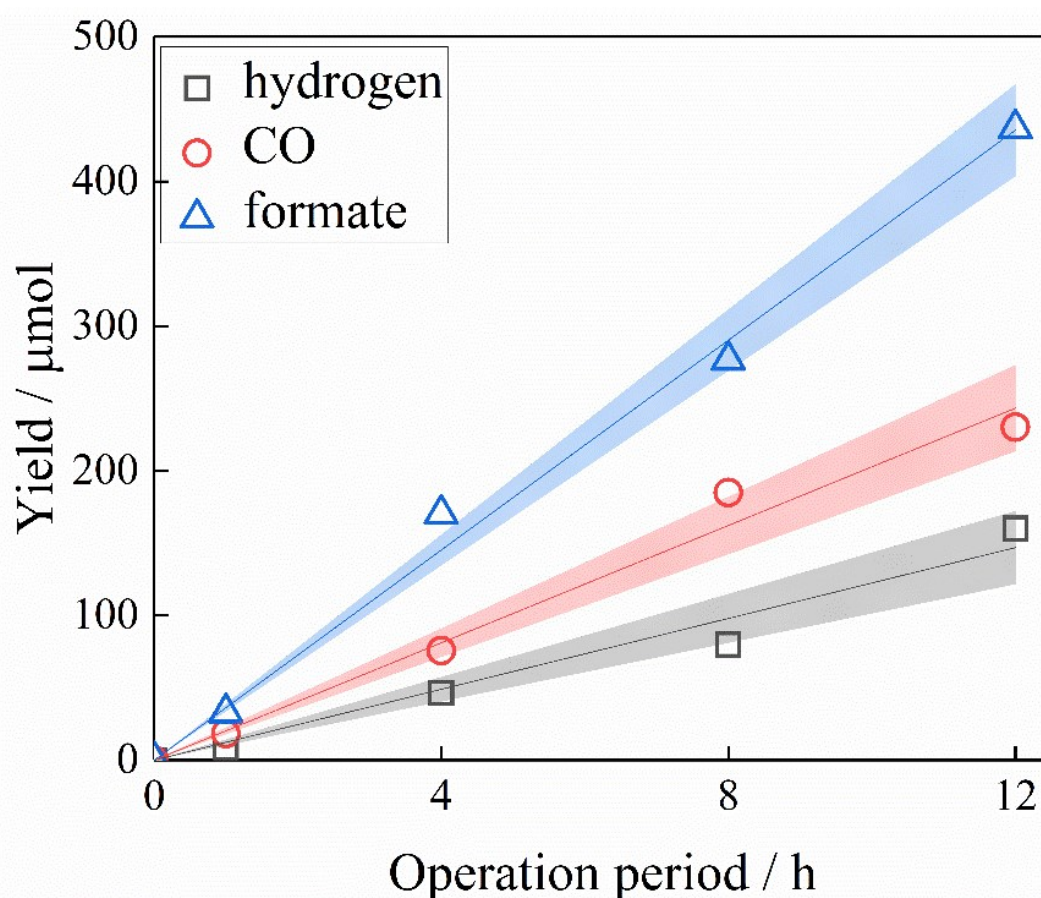
Figure S6. Variations of the yields of hydrogen, CO and formate with time and corresponding proportional fittings. Shaded regions represent 95% confidence band. OP-Cu-catalyzed PEC CO_2R reactions were performed for 50 atm and for the photoanode potential of ~0.4 V versus the Ag/AgCl reference. The operation periods are 1, 4, 8 and 12 hours.
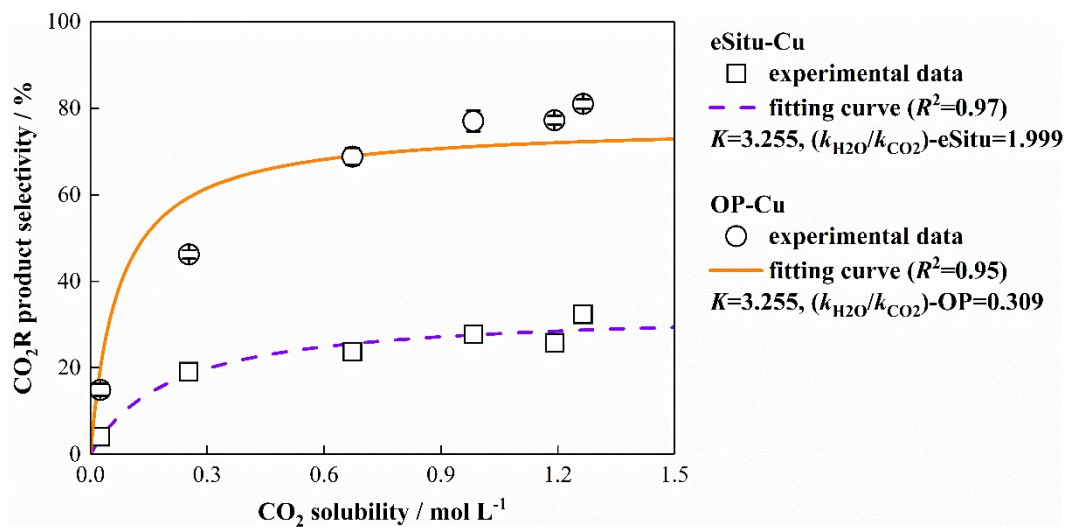
Figure S7. Variations of CO_2R product selectivity with CO_2 solubility in 0.1 M $KHCO_3$ electrolyte and corresponding Langmuir mechanism fittings for eSitu-Cu and OP-Cu.
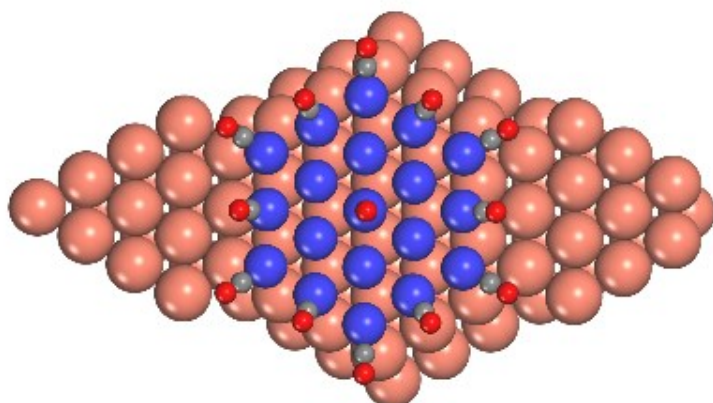
Figure S8. DFT calculation results. The formation of Cu nanoclusters has been reported for the Cu surface exposed to small amount of CO [21]. These nanoclusters increase the concentration of active sites for CO_2R [22]. Here, as an example, we further provided evidence for the formation of a nanocluster comprising 19 Cu atoms with 13 adsorbed CO molecules by DFT calculations. All the DFT calculations were performed using the Vienna Ab-initio Simulation Package (VASP) where PBE+U method was used. The dimensions of the four-atomic-layer Cu (111) surface with a nanocluster is 7×7×4. The 3×3×1 Monkhorst-Pack mesh was used for k-point sampling. The calculated adsorption energy for CO adsorption on top-sites of Cu (111) is -0.45 eV, which agrees with experimental data in literature. Calculations show that the average CO adsorption energy for edge and corner sites is -0.79 eV and the formation energy of a 19-Cu-atom cluster is 3.82 eV. These results indicate that the formation is favorable for the above-shown optimized structure, a 19-Cu-atom cluster with 12 CO molecules adsorbed on edge and corner sites.
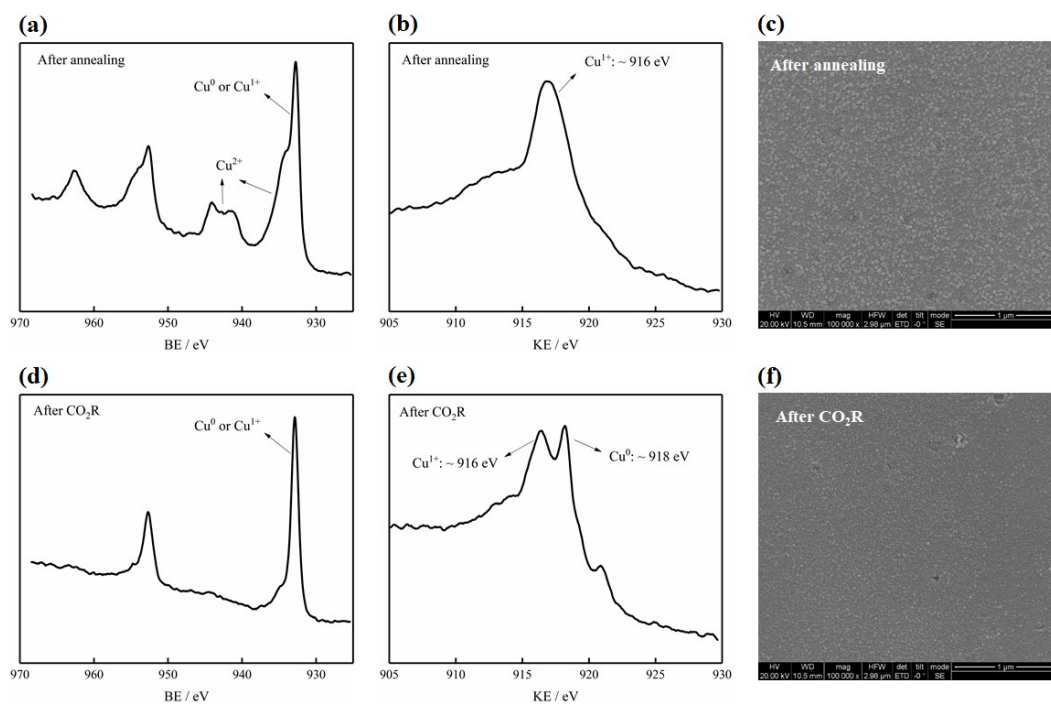
Figure S9. Characterizations of the Cu_2O precursor and OP-Cu. (a) and (b) XPS spectra

and (c) SEM image of the Cu_2O precursor. (d) and (e) XPS spectra and (f) SEM image
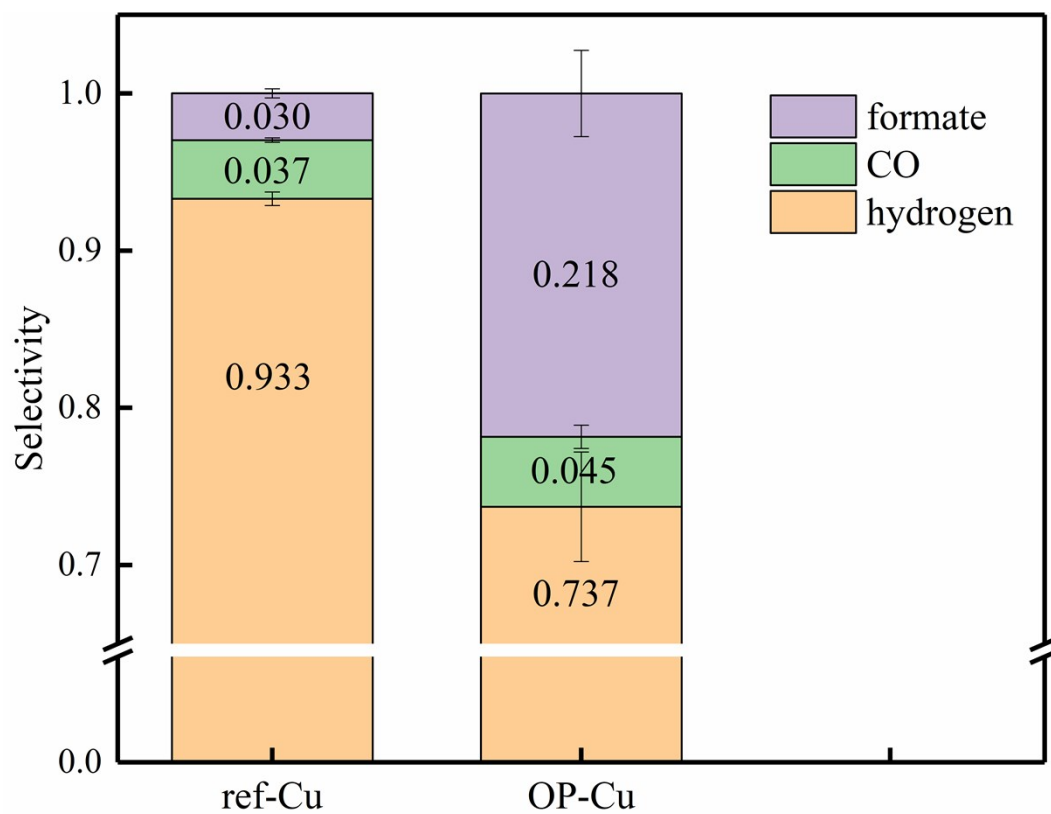
of OP-Cu.

Figure S10. Product selectivity of ref-Cu and OP-Cu. Gaseous products are hydrogen and CO, and liquid product is formate.
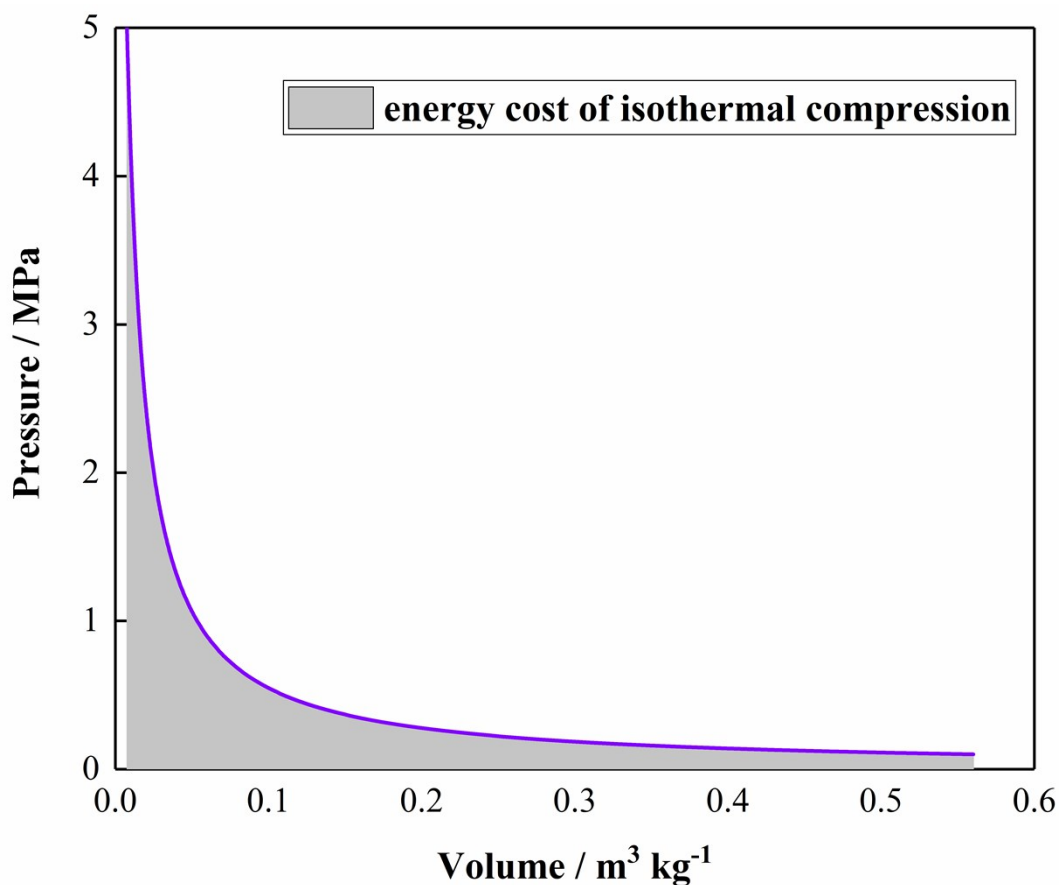
Figure S11. Variation of CO_2 pressure with CO_2 volume at 298 K taken from the NIST database. We have calculated the energy that is needed for the process of pressurizing one mole of CO_2 from ambient to 50 atm. This process can be regarded as isothermal compression, so the energy is calculated by integrating the $p(v)$ function (variation of CO_2 pressure with CO_2 volume) from ambient CO_2 volume to the volume at 50 atm. The calculated energy is 222.8 J g^{-1} CO_2, *i.e.* 9.8 kJ mol^{-1} CO_2. The chemical energy is 256.6 kJ mol^{-1} for CO and 285.6 kJ mol^{-1} for formate. These results show that the input compression energy is less than 4% of the output chemical energy. Therefore, the energy cost of pressurization can be neglected.
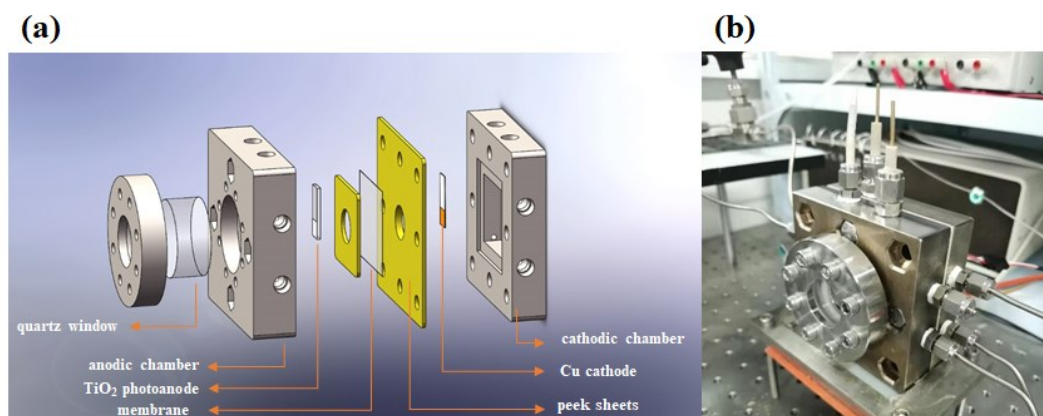
Figure S12. Details of the high-pressure reactor. (a) Assembly and (b) photo of the reactor. The customized reactor with three electrodes inside was made of stainless steel coated with Teflon for electrical insulation. The dimensions are 1cm×4cm×4cm for both the anodic and the cathodic chambers.

Table S1. Product analysis after the first 15 minutes for OP-Cu at 10 atm

Parameter	Value	Parameter	Value
H_2 yield (μmol)	1.2	H_2 Faradaic efficiency (%)	7.6
CO yield (μmol)	1.8	CO Faradaic efficiency (%)	11.8
Formate yield (μmol)	0.7	Formate Faradaic efficiency (%)	4.6
Total charges (C)	3.0	Total Faradaic efficiency (%)	24.0[a]

[a]Large amount of charges were consumed by Cu_2O reduction

Table S2. Product analysis over the next 45 minutes for OP-Cu at 10 atm

Parameter	Value	Parameter	Value
H_2 yield (μmol)	28.1	H_2 Faradaic efficiency (%)	52.1
CO yield (μmol)	11.3	CO Faradaic efficiency (%)	20.9
Formate yield (μmol)	10.6	Formate Faradaic efficiency (%)	19.7
Total charges (C)	10.4	Total Faradaic efficiency (%)	92.7

Table S3. Summary of Auger parameters and atomic ratios of each copper oxidation state for OP-Cu (1h), OP-Cu (12h) and Cu foil.

Sample	Oxidation state	Cu 2p (eV)	Cu LMM (eV)	Auger parameters (eV)	Ratio (%)
OP-Cu (1h)	Cu^0	932.60	918.95	1851.55	36.11
	Cu^{1+}	932.60	916.80	1849.40	63.89
OP-Cu (12h)	Cu^0	932.50	918.95	1851.45	36.19
	Cu^{1+}	932.50	916.80	1849.30	63.81
Cu foil	Cu^0	932.60	918.55	1851.15	38.78
	Cu^{1+}	932.60	916.70	1849.30	48.40
	Cu^{2+}	934.35	917.90	1852.25	12.82

Table S4. CO_2R Performance of HiPAD during one hour for various pressures

Pressure (atm)	H_2 yield (μmol)	CO yield (μmol)	Formate yield (μmol)	Solar-to-chemical efficiency (%)
1	46.2	3.2	5.5	0.74
10	29.3	13.1	11.4	0.75
30	15.2	15.5	20.5	0.75
50	12.2	25.6	19.7	0.84
70	13.6	22.9	21.3	0.84
90	12.4	22.9	27.5	0.93

Table S5. Performance comparison of photoelectrochemical CO_2 reduction

References	CO_2R selectivity	Efficiency
This work	80%	0.93%[a]
Energ. Environ. Sci. 2020, online	75%	0.19%[a]
Energ. Environ. Sci. 2019, 12, 923	50%	0.29%[a]
Energ. Environ. Sci. 2019, 12, 923	50%	0.42%[b]
J. Am. Chem. Soc. 2018, 140, 7869	20%	0.87%[b]
J. Am. Chem. Soc. 2018, 140, 7869	80%	~ 0.4%[b]

[a]Solar-to-chemical energy conversion efficiency

[b]Half-cell efficiency or the applied bias photon-to-current efficiency

Table S6. Performance of HiPAD for 50 atm and 1-sun condition

Parameter	Value	Parameter	Value
H_2 yield (μmol)	12.8	H_2 Faradaic efficiency (%)	51.2
CO yield (μmol)	1.4	CO Faradaic efficiency (%)	5.5
Formate yield (μmol)	8.3	Formate Faradaic efficiency (%)	33.2
Acetate yield (μmol)	0.3	Acetate Faradaic efficiency (%)	5.2
Total charges (C)	4.8	Total Faradaic efficiency (%)	95.0
PEC CO_2R time (s)	5215	Solar-to-chemical efficiency (%)	1.16

References

[S1] M. C. Biesinger, Surf. Interface Anal. 2017, 49, 1325-1334.

[S2] M. Shima, K. Tsutsumi, A. Tanaka, H. Onodera, M. Tanemura, Surf. Interface Anal. 2018, 50, 1187-1190.